Bifurcations in a parametrically forced magnetic pendulum

Sang-Yoon Kim,* Seung-Ho Shin, Jaichul Yi, and Chi-Woong Jang
Department of Physics, Kangwon National University, Chunchon, Kangwon-Do 200-701, Korea
(Received 17 July 1997)

An experimental study of bifurcations associated with the stability of stationary points (SP's) in a parametrically forced magnetic pendulum, and a comparison of its results with numerical results, are presented. The critical values for which the SP's lose or gain their stability are experimentally measured by varying the two parameters Ω (the normalized natural frequency) and A (the normalized driving amplitude). It is observed that, when the amplitude A exceeds a critical value, the normal SP with $\theta=0$ (θ is the angle between the permanent magnet and the magnetic field) becomes unstable either by a period-doubling bifurcation or by a symmetry-breaking pitchfork bifurcation, depending on the values of Ω. However, in contrast with the normal SP the inverted SP, with $\theta=\pi$ is observed to become stable as A is increased above a critical value by a pitchfork bifurcation, but it also destabilizes for a higher critical value of A by a period-doubling bifurcation. All of these experimental results agree well with numerical results obtained using the Floquet theory.
[S1063-651X(97)06212-0]

PACS number(s): 05.45.+b, 03.20.+i

I. INTRODUCTION

We consider a permanent magnet of dipole moment m placed in a periodically time-varying magnetic field B [1–3]. Its motion can be described by a second-order nonautonomous ordinary differential equation,

$$I\ddot{\theta}+b\dot{\theta}+m(B_{\rm dc}+B_{\rm ac}\sin\omega t)\sin\theta=0, \tag{1}$$

where the overdot denotes the differentiation with respect to time, θ is the angle between the magnet and the magnetic field, I is the moment of inertia about a rotation axis, b is the damping parameter, $B_{\rm dc}$ is the steady dc componet of B, and $B_{\rm ac}$ and ω are the amplitude and frequency of the sinusoidally time-varying ac component of B, respectively. Making the normalization $\omega t\rightarrow 2\pi t$ and $\theta\rightarrow 2\pi x$, we have

$$\ddot{x}+2\pi\gamma\dot{x}+2\pi(\Omega^2+A\sin 2\pi t)\sin 2\pi x=0, \tag{2}$$

where $\omega_0=\sqrt{mB_{\rm dc}/I}$, $\Omega=\omega_0/\omega$, $\gamma=b/I\omega$, and $A=mB_{ac}/I\omega^2$. Note that this is just a normalized equation of motion for the parametrically forced gravitational pendulum with a vertically oscillating support [4–9]. Hence this magnetic system can be taken as a model of the parametrically forced pendulum equation. Hereafter we will call this magnetic oscillator a parametrically forced magnetic pendulum.

The parametrically forced pendulum, albeit simple looking, shows a richness in its dynamical behavior. As the normalized driving amplitude A is increased, transitions from periodic attractors to chaotic attractors, and vice versa, coexistence of different attractors, transient chaos, multiple period-doubling transitions to chaos, and so on have been numerically found [5–7]. Some of them have also been observed in real experiments on the parametrically forced magnetic pendulum [1–3] and gravitational pendulum [8,9]. However, so far only the case of $\Omega=0$ (i.e., the case $B_{\rm dc}=0$) has been studied in experiments on the magnetic pendulum.

In this paper, we experimentally study bifurcations associated with the stability of the stationary points (SP's) in the parametrically forced magnetic pendulum by varying the normalized natural frequency Ω and the normalized driving amplitude A, and then compare the experimental results with the numerical results obtained using the Floquet theory [10]. We first note that the magnetic pendulum has two SP's. One is the ''normal'' SP with $(x,\dot{x})=(0,0)$, and the other one is the ''inverted'' SP with $(x,\dot{x})=(\frac{1}{2},0)$. For the case of the ''unforced'' simple magnetic pendulum (with $A=0$), the normal SP is stable, while the inverted SP is unstable. However, as A is increased above a critical value, the normal SP loses its stability. Using the Floquet theory, bifurcations occurring at such critical values have been numerically studied by one of us (Kim) and Lee [7]. In contrast to the normal SP, the inverted SP gains its stability when A exceeds a critical value [11–15]. We also study numerically bifurcations associated with stability of the inverted SP using the Floquet theory for a comparison with the experimental results.

This paper is organized as follows. We first explain the experimental setup for the parametrically forced magnetic pendulum in Sec. II. Bifurcations of the two SP's are then experimentally investigated in Sec. III. It is observed that as A is increased beyond a critical value, the normal SP loses its stability either by a period-doubling bifurcation or by a symmetry-breaking pitchfork bifurcation, depending on the values of Ω. For the case of the period-doubling bifurcation, a new stable symmetric orbit with period 2 is born, while for the case of the symmetry-breaking pitchfork bifurcation a conjugate pair of new stable asymmetric orbits with period 1 appears. In contrast to the normal SP, the inverted SP is observed to gain its stability when A exceeds a first critical value A_1^* by a pitchfork bifurcation, but it also destabilizes for a higher second critical value A_2^* of A by a period-doubling bifurcation. Thus the inverted SP becomes stable in the interval between A_1^* and A_2^*. Our experimental data

*Electronic address: sykim@cc.kangwon.ac.kr

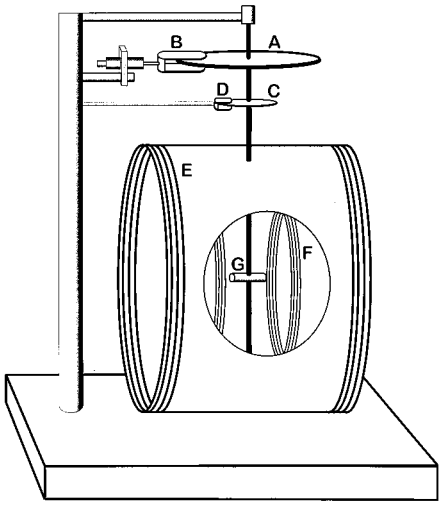

FIG. 1. Exploded view of a parametrically forced magnetic pendulum. Labeled components are the aluminum damping plate (A), the horseshoe magnet controlled by a micrometer (B), the code wheel (C), the encoder module (D), the Helmholtz coil for production of a steady dc component of a spatially uniform magnetic field B (E), the Helmholtz coil for production of a sinusoidally time-varying ac component of B (F), and the permanent bar magnet (G).

show a good agreement between experimental and numerical results. Finally, Sec. IV gives a summary.

II. EXPERIMENTAL SETUP

An exploded view of the experimental apparatus is shown in Fig. 1. The physical magnetic pendulum consists of a permanent bar magnet, an aluminum damping plate, and a code wheel, which are coaxially attached to a rotation axis. This magnetic pendulum shows rich dynamical behavior in a periodically time-varying magnetic field B, generated by Helmholtz coils. Each component of the apparatus is explained in some detail below.

A permanent bar magnet, glued to a rotation axis guided by a small ball in the lowest part, and by a tiny pin in the highest part, is placed in the center of two sets of Helmholtz coils, producing the magnetic field B perpendicular to the rotation axis. The number of turns N and the radius R for a large set of Helmholtz coils are $N=130$ and $R=10.8$ cm, while they are $N=144$ and $R=5.8$ cm for a smaller set of Helmholtz coils. The large set of Helmholtz coils is given a direct current $I_{\rm dc}$ to supply a steady dc component $B_{\rm dc}$ of B. On the other hand, the smaller set of Helmholtz coils, which is nested inside the large set and driven by a Pasco model CI-6552A ac power amplifier, provides a sinusoidally time-varying ac component of B with amplitude $B_{\rm ac}$ and frequecny ω. This amplifier can handle currents up to 1 A. Since higher currents are necessary in some range of Ω, we also use a current booster to increase the current up to 2 A.

We take into account the effect of the normal component $B_{E,n}$ of the Earth's magnetic field B_E perpendicular to the rotation axis, and align both dc and ac components of the applied magnetic field B parallel to $B_{E,n}$. The angle of the permanent bar magnet is experimentally measured from this aligned direction (i.e., the direction of $B_{E,n}$). Since the effective dc component $B_{\rm eff}$ of the total magnetic field is given by $B_{\rm eff}=B_{\rm dc}+B_{E,n}$, the natural frequency ω_0 in Eq. (2) becomes $\omega_0=\sqrt{(m/I)B_{\rm eff}}$, where $m/I=2.542\ {\rm G}^{-1}\,{\rm s}^{-2}$ and $B_{E,n}=0.223$ G [16].

A damping force proportional to the angular velocity can be supplied by an eddy current brake. Such eddy-current damping is adjusted by controlling the separation between the aluminum damping plate and the horseshoe magnet with a micrometer screw. It is also possible to determine a damping parameter k ($\equiv b/2I$) and the natural frequency ω_0 by fitting a sampled time series $\theta(t)$ for the unforced case of $B_{\rm ac}=0$ to an equation, $\theta(t)=Ce^{-kt}\cos(\sqrt{\omega_0^2-k^2}\,t+\delta)$ (C and δ are some constants), which is just the angle in the case of the underdamped motion of the unforced magnetic pendulum for small angular displacements.

For data acquisition and experimental control, we use commercial products ''Rotary Motion Sensor'' and ''Signal Interface,'' manufactured by the Pasco Scientific. A Pasco model CI-6538 rotary motion sensor set consists of a code wheel with 1440 slots (i.e., a disk with an angular code in the form of sectors which are pervious or impervious to light) and an encoder module containing a light-emitting diode (LED) and two photodiodes with signal-processing circuitry. As the code wheel moves, the light signal emitted from the LED is interrupted by the slots, and electrically encoded. Thus a code wheel with 1440 slots can generate raw data with a resolution of $\Delta\theta=0.004$ rad. A personal computer equipped with a Pasco model CI-6560 signal interface unit analyzes the signals from the rotary motion sensor and provides an easy-to-use data set of $(\theta,\dot{\theta})$ at a chosen sampling rate. It also performs a convenient experimental control.

III. BIFURCATIONS OF THE NORMAL AND INVERTED SP'S

In this section we first analyze the bifurcations associated with stability of the SP's in the parametrically forced magnetic pendulum, using the Floquet theory. The experimental results for the cases of the normal and inverted SP's are then presented and compared with the numerical results.

A. Bifurcation analysis based on the Floquet theory

The normalized second order ordinary differential equation (2) is reduced to two first order ordinary differential equations

$$\dot{x}=y, \tag{3a}$$

$$\dot{y}=-2\pi\gamma y-2\pi(\Omega^2+A\sin 2\pi t)\sin 2\pi x. \tag{3b}$$

These equations have an inversion symmetry S, since the transformation

$$S: x\to -x,\ \ y\to -y,\ \ t\to t \tag{4}$$

leaves Eq. (3) invariant. If an orbit $z(t)$ [$\equiv(x(t),y(t))$] is invariant under S, it is called a symmetric orbit. Otherwise, it is called an asymmetric orbit, and has its ''conjugate'' orbit $Sz(t)$ [$=(-x(t),-y(t))$].

The Poincaré maps of an initial point z_0 $[=(x(0),y(0))]$ can be computed by sampling the orbit points z_m at the discrete time $t=m$, where $m=1,2,3,\ldots$. We call the transformation $z_m \rightarrow z_{m+1}$ the Poincaré (time-1) map, and write $z_{m+1}=P(z_m)$. Note that the normal and inverted SP's of the parametrically forced magnetic pendulum, denoted by $\hat{z}_N$ $[\equiv(0,0)]$ and $\hat{z}_I$ $[\equiv(\frac{1}{2},0)]$, respectively, are the fixed points of the Poincaré map P [i.e., $P(\hat{z})=\hat{z}$ $(\hat{z}=\hat{z}_N,\hat{z}_I)$] with period 1.

Here we investigate bifurcations associated with stability of the two normal and inverted fixed points of P. The linear stability of a fixed point is determined from the linearized-map matrix M of P at $\hat{z}$. Using the Floquet theory [10], we obtain the matrix M by integrating the linearized differential equations for small perturbations as follows. Consider an infinitesimal perturbation $[\delta x(t),\delta y(t)]$ to a SP. Linearizing Eq. (3) about the SP, we obtain

$$\begin{pmatrix} \delta\dot{x} \\ \delta\dot{y} \end{pmatrix} = J(t) \begin{pmatrix} \delta x \\ \delta y \end{pmatrix}, \tag{5}$$

where

$$J(t)=\begin{pmatrix} 0 & 1 \\ -4\pi^2(\Omega^2+A\sin 2\pi t)\cos 2\pi\hat{x} & -2\pi\gamma \end{pmatrix}. \tag{6}$$

Here $\hat{x}=0$ and $\frac{1}{2}$ for the normal and inverted SP's, respectively. Note that J is a 2×2 1-periodic matrix [i.e., $J(t+1)=J(t)$]. Let $W(t)=[w^1(t),w^2(t)]$ be a fundamental solution matrix with $W(0)=I$. Here $w^1(t)$ and $w^2(t)$ are two independent solutions expressed in column vector forms, and I is the 2×2 unit matrix. Then a general solution of the 1-periodic system has the following form:

$$\begin{pmatrix} \delta x(t) \\ \delta y(t) \end{pmatrix} = W(t) \begin{pmatrix} \delta x(0) \\ \delta y(0) \end{pmatrix}. \tag{7}$$

Substitution of Eq. (7) into Eq. (5) leads to an initial-value problem in determining $W(t)$:

$$\dot{W}(t)=J(t)W(t), \quad W(0)=I. \tag{8}$$

It is clear from Eq. (7) that $W(1)$ is just the linearized-map matrix M. Hence the matrix M can be obtained through numerical integration of Eq. (8) over the period 1.

The characteristic equation of the numerically obtained M is

$$\lambda^2-\mathrm{tr}M\lambda+\det M=0, \tag{9}$$

where tr$M$ and det$M$ denote the trace and determinant of M, respectively. The eigenvalues λ_1 and λ_2 of M are called the Floquet (stability) multipliers, characterizing the stability of the fixed point. It was also shown in Ref. [17] that the determinant of M is given by $\det M=e^{-2\pi\gamma}$. Hence the pair of Floquet multipliers of the fixed point lies either on the circle of radius $e^{-\pi\gamma}$ or on the real axis in the complex plane. The fixed point is stable only when both Floquet multipliers lie inside the unit circle. We first note that they never cross the unit circle except at the real axis (i.e., they never have complex values with moduli larger than unity), and hence Hopf bifurcations do not occur. Consequently, the fixed point can lose its stability only when a Floquet multiplier λ decreases (increases) through -1 (1) on the real axis.

When a Floquet multiplier λ decreases through -1, the fixed point loses its stability via period-doubling bifurcation, which leads to the birth of a new stable symmetric orbit with period 2. On the other hand, when a Floquet multiplier λ increases through 1, it becomes unstable via pitchfork bifurcation, which results in the birth of a conjugate pair of stable asymmetric orbits with period 1. Since the newly born orbits are asymmetric ones, the pitchfork bifurcation is also called a symmetry-breaking bifurcation. For more details on bifurcations, refer to Ref. [18].

The stability boundaries of the normal and inverted SP's in some ranges of the Ω-A plane are determined through numerical calculations of their Floquet multipliers λ's. The absolute value of λ at such stability boundaries is 1 (i.e., $|\lambda|=1$). If $\lambda=-1$, then the boundary is a period-doubling bifurcation line. Otherwise, it is a symmetry-breaking pitchfork bifurcation line. We also obtain the bifurcation diagrams and the phase-flow and Poincaré-map plots numerically at some chosen parameter values for clear visual representation of the bifurcations. All of these numerical results are given in the next two subsections (see Figs. 2–7) for a comparison with the experimental results.

B. Experimental results for the case of the normal SP

In all the experiments for normal and inverted SP's, we fix the the driving frequency ω in Eq. (1), and the normalized damping parameter γ in Eq. (2), as $\omega=2\pi$ and $\gamma=0.1$, respectively. We then control the normalized natural frequency and driving amplitude Ω and A in Eq. (2) by varying B_{dc} and B_{ac}, respectively, and study the bifurcations of the two SP's.

We consider two ranges of Ω for the normal SP, I:$0.2\leqslant\Omega\leqslant 0.5$ and II:$0.8\leqslant\Omega\leqslant 1.025$. For each chosen value of Ω, we increase the amplitude A, and observe whether the SP is stable or not. In order to determine the stability of the SP experimentally, we release the magnetic pendulum from rest at a small initial angle displaced from the SP. If the SP is stable, then the subsequent motion damps toward the SP. Otherwise, it deviates from the SP. Thus we measure a critical value A^*_{expt} of A experimentally, above which the SP is unstable.

We first study the bifurcations of the normal SP in the first range I of Ω. As an example, consider the case of $\Omega=0.4$. With increasing A, we carry out the experiments, and measure the critical value A^*_{expt}. It is observed that for $A>A^*_{\mathrm{expt}}$, the SP becomes unstable through a period-doubling bifurcation, giving rise to the birth of a new stable symmetric period-doubled orbit. For a visual representation of the bifurcation, we obtain the bifurcation diagram and the phase-flow and Poincaré-map plots below.

For phase representation, we acquire a data set of $[\theta(t),\dot{\theta}(t)]$ at a fixed sampling rate of 20 Hz, and convert it into a normalized set of (x,y). This whole set of the data is used for a phase-flow plot, while a partial set of the data chosen at integral multiples of the external driving period T $(=2\pi)$ [i.e., $t=nT$ $(n=0,1,2,\ldots)$] is used for a Poincaré-map plot and for a bifurcation diagram.

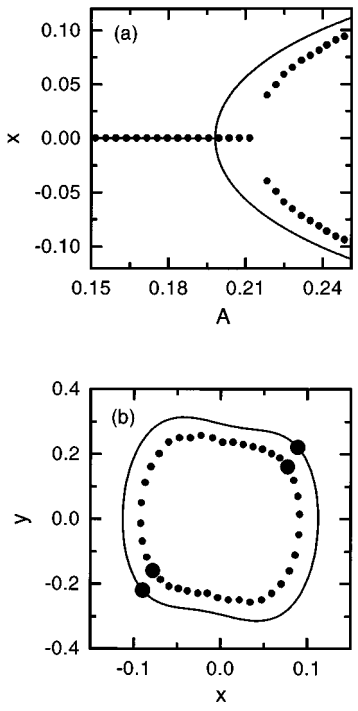

FIG. 2. Period-doubling bifurcation of the normal SP for $\Omega = 0.4$. As shown in the bifurcation diagram (a), the normal SP denoted by the solid circles becomes unstable for a critical value A^*_{expt} ($=0.215$) by a period-doubling bifurcation, which results in the birth of a symmetric period-doubled orbit denoted by the solid circles. The experimental data for the phase flow for $A = 0.23$ are denoted by the small solid circles in (b). Numerical data denoted by the solid lines are also given in both (a) and (b). The data for the Poincaré maps in (b) are represented by the two large solid circles for both the experimental and numerical cases. For more details, see the text.

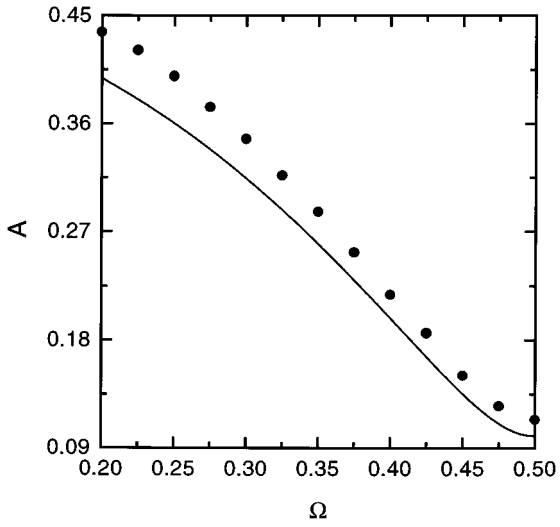

FIG. 3. Stability diagram of the normal SP in the 1st range I of Ω (i.e., $0.2 \leqslant \Omega \leqslant 0.5$). The experimental data for the critical values A^*_{expt}'s, above which the SP becomes unstable, are represented by the solid circles. The stability boundary numerically determined using the Floquet theory is denoted by the solid line, and it is just a period-doubling bifurcation line.

The bifurcation diagram for $\Omega = 0.4$ is shown in Fig. 2(a). The data obtained through numerical calculations are also given for a comaprison with the experimental results. Note that for the bifurcation diagram, the experimental data represented by the solid circles agree well with the numerical data denoted by the solid lines. For reference, the critical values obtained through experiments and numerical calculations are $A^*_{\text{expt}} = 0.215$ and $A^*_{\text{nu}} = 0.198\,131\ldots$, respectively. As A is increased above the critical value A^*, the normal SP loses its stability via period-doubling bifurcation, and a new stable symmetric period-doubled orbit appears. Figure 2(b) shows the phase-flow and Poincaré-map plots of the symmetric period-doubled orbit for $A = 0.23$. The experimental data for the phase flow are represented by the small solid circles, while the two larger solid circles denote the experimental data for the Poincaré map. These experimental data are also in a good agreement with the numerically computed data for the phase flow represented by the solid line and for the Poincaré map denoted by the two large circles.

We also perform the above experiments for many other values of Ω in the first range I, and thus measure the critical values A^*_{expt}'s. The stability diagram of the normal SP is shown in Fig. 3. The experimental data for A^*_{expt} are represented by the solid circles, and they seem to lie on a smooth stability boundary curve. For a comparison with the experimental data, the stability boundary of the SP numerically calculated using the Floquet theory is also denoted by the solid line in Fig. 3. This stability boundary is just a period-doubling bifurcation line at which a Floquet multiplier of the SP is $\lambda = -1$. The period-doubling bifurcation line determined through numerical computations lies a little below that experimentally determined. That is, the value of A^*_{expt} is somewhat higher than that of A^*_{nu}. This is what one would expect, because in real experiments there exists a frictional force due to a contact between the rotation axis and its guiders (ball and pin). As previously noted [8,9], one of the main effects of this frictional force is to make the origin of the phase plane (i.e., the normal SP) stable up to higher values of the external driving amplitude than the numerically calculated critical value A^*_{nu}.

We now study the bifurcations of the normal SP in the second range II of Ω (i.e., $0.8 \leqslant \Omega \leqslant 1.025$). As in the above first range I of Ω, we increase the amplitude A and measure a critical value A^*_{expt}, beyond which the SP becomes unstable, by releasing the magnetic pendulum from rest at a small initial angle displaced from the SP. However, in contrast to the first range of Ω the normal SP is observed to lose its stability through a symmetry-breaking pitchfork bifurcation for $A = A^*_{\text{expt}}$, which leads to the birth of a conjugate pair of new stable asymmetric orbits with period 1.

As an example, consider the case of $\Omega = 0.95$. The bifurcation diagram for this case is shown in Fig. 4(a). The normal SP denoted by the solid circles is observed to become unstable through a symmetry-breaking pitchfork bifurcation for $A^*_{\text{expt}} = 1.25$. For $A > A^*_{\text{expt}}$, a pair of stable asymmetric orbits of period 1 appears. One is represented by the solid circles, while its conjugate orbit is denoted by the open circles. Figure 4(b) shows the phase-flow and Poincaré-map plots of a conjugate pair of symmetry-broken orbits of period 1 for $A = 1.4$. The small solid circles denote the phase flow

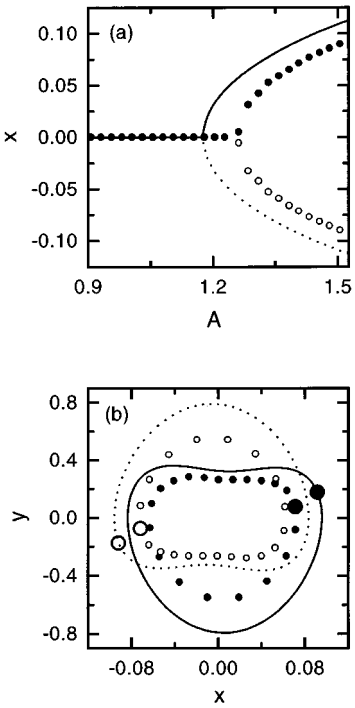

FIG. 4. Symmetry-breaking pitchfork bifurcation of the normal SP for $\Omega=0.95$. For a critical value $A^*_{\rm expt}$ $(=1.25)$, the normal SP denoted by the solid circles becomes unstable by a symmetry-breaking pitchfork bifurcation, as shown in the bifurcation diagram (a). As a result of the bifurcation, a conjugate pair of asymmetric orbits of period 1 appears; one is denoted by the solid circles, while the other one is represented by the open circles. The experimental data for the phase flow of the two symmetry-broken orbits for $A=1.4$ are denoted by the small solid and open circles in (b), respectively. Numerical data for the two symmetry-broken orbits are also given in both (a) and (b); one is denoted by the solid line, while the other one is represented by the dotted line. The data for the Poincaré maps in (b) are represented by the large solid and open circles for both the experimental and numerical cases. For more details, see the text.

of an asymmetric ''heart-shaped'' orbit, while the small open circles represent the phase flow of its conjugate ''inverted heart-shaped'' orbit. The data for the Poincaré maps of the two symmetry-broken orbits are also denoted by the larger solid and open circles, respectively. This symmery-broken case is in contrast to the symmetry-preserved case [see Fig. 2(b)] in the first range of Ω. For a comparison with the experimental results, the data obtained by numerical computations are also given in Fig. 4. As A is increased above a critical value $A^*_{\rm nu}$ $(=1.174\,209\ldots)$, the normal SP denoted by the solid line becomes unstable through a symmetry-breaking pitchfork bifurcation, giving rise to the birth of a conjugate pair of symmetry-broken orbits of period 1. One asymmetric orbit is represented by the solid line, while the other one is denoted by the dotted line. As in the experimental case, the data for the Poincaré maps of the two asymmetric orbits are denoted by the large solid and open circles, respectively. All of these experimental and numerical results seem to agree well.

We also measure the critical values $A^*_{\rm expt}$'s for many other values of Ω in the second range II. Figure 5 shows the stability diagram for this case. The experimental data for $A^*_{\rm expt}$ are denoted by the solid circles, while the stability boundary numerically computed using the Floquet theory is represented by the solid line. In contrast to the first range of Ω, the stability boundary is a symmetry-breaking pitchfork bifurcation line at which a Floquet multiplier of the SP is $\lambda=1$. We also note that as in the case of the first range I, the value of $A^*_{\rm expt}$ is somewhat higher than that of $A^*_{\rm nu}$ because of the frictional force between the rotation axis and its guiders.

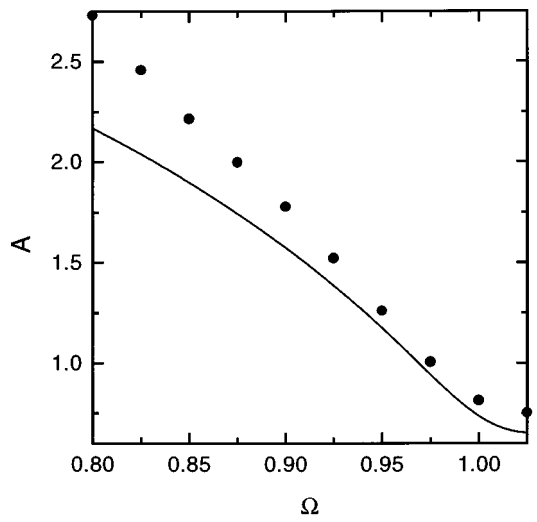

FIG. 5. Stability diagram of the normal SP in the second range II of Ω (i.e., $0.8\leqslant\Omega\leqslant1.025$). The experimental data for the critical values $A^*_{\rm expt}$'s, above which the SP becomes unstable, are represented by the solid circles. The stability boundary numerically determined using the Floquet theory is denoted by the solid line, and it is just a symmetry-breaking pitchfork bifurcation line.

C. Experimental results for the case of the inverted SP

In this subsection, we study the bifurcations associated with stability of the inverted SP by increasing A in a range of $0.2\leqslant\Omega\leqslant0.5$. In contrast to the normal SP, the inverted SP is observed to gain its stability when a 1st critical value A^*_1 of A is exceeded by a subcritical pitchfork bifurcation. However, as A is further increased, the stabilized inverted SP is also observed to lose its stability for a second critical value A^*_2 of A through a period-doubling bifurcation. Thus the inverted SP becomes stable in the interval between A^*_1 and A^*_2.

As an example, we consider the case of $\Omega=0.2$. The bifurcation diagram for this case is shown in Fig. 6(a). The unstable inverted SP denoted by the open circles is observed to become stable when A is increased above a 1st critical value $A^*_{\rm expt,1}$ $(=0.39)$. Using the Floquet theory, the unstable inverted SP denoted by the dashed line is also numerically found to gain its stability for $A>A^*_{\rm nu,1}$ $(=0.289\,108\ldots)$ by a subcritical pitchfork bifurcation, giving rise to the birth of a conjugate pair of unstable asymmetric orbits with period 1, denoted by the dashed lines. However, unfortunately the two symmetry-broken orbits born for this subcritical case cannot be experimentally observed, because they are unstable ones. This is in contrast to the supercritical bifurcations occurring for the normal SP in the second range II of Ω (for a super-

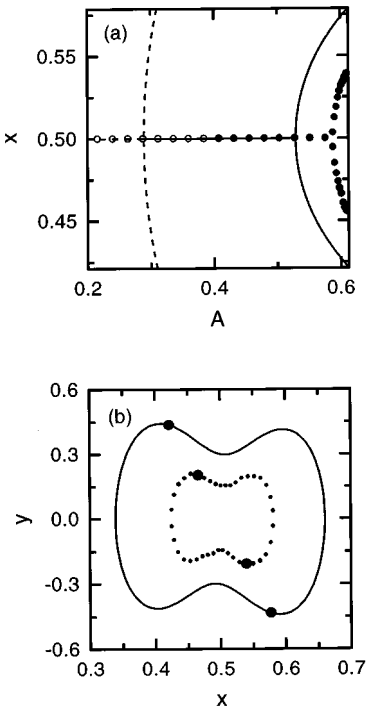

FIG. 6. Bifurcations of the inverted SP for $\Omega=0.2$. The bifurcation diagram for $\Omega=0.2$ is shown in (a). In contrast to the normal SP, the inverted SP denoted by the open circles is observed to become stable as A is increased above a 1st critical value $A^*_{\mathrm{expt},1}$ $(=0.39)$. However, as A is further increased, the stabilized inverted SP denoted by the solid circles is also observed to lose its stability for a second critical value $A^*_{\mathrm{expt},2}$ $(=0.567)$ through a period-doubling bifurcation, giving rise to the birth of a symmetric period-doubled orbit denoted by the solid circles. The experimental data for the phase flow of the period-doubled orbit for $A=0.61$ are denoted by the small solid circles in (b). Numerical data denoted by the lines are also given in both (a) and (b); a stable orbit is denoted by a solid line, while an unstable orbit is represented by a dashed line. The data for the Poincaré maps in (b) are represented by the two large solid circles for both the experimental and numerical cases. For more details, see the text.

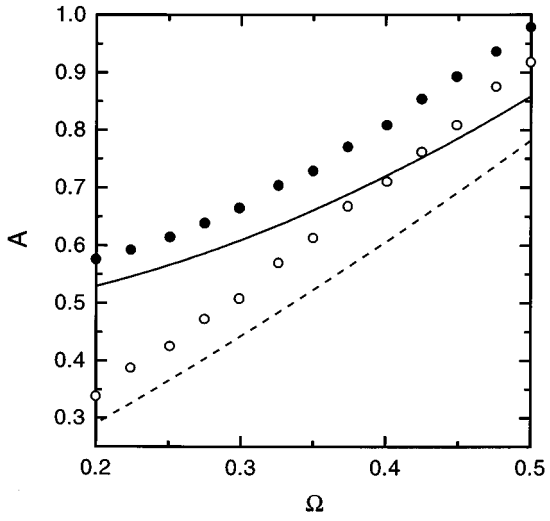

FIG. 7. Stability diagram of the inverted SP in the range of $0.2\leqslant\Omega\leqslant0.5$. The experimental data for the first and second critical values, $A^*_{\mathrm{expt},1}$ and $A^*_{\mathrm{expt},2}$, are represented by the open and solid circles, respectively. The lower and upper stability boundaries, numerically computed using the Floquet theory and denoted by the dashed and solid lines, are the symmetry-breaking pitchfork and period-doubling bifurcation lines, respectively.

critical case, a pair of stable asymmetric orbits is born, which can be experimentally observed as shown in Fig. 4). As A is further increased from $A^*_{\mathrm{expt},1}$, the stabilized inverted SP denoted by the solid circles is observed to lose its stability by a period-doubling bifurcation when a second critical value $A^*_{\mathrm{expt},2}$ $(=0.567)$ is exceeded. For $A>A^*_{\mathrm{expt},2}$, a stable symmetric ''butterfly-shaped'' orbit of period 2 appears. Small solid circles and the two larger solid circles in Fig. 6(b) represent the phase flow and Poincaré map of the symmetric orbit of period 2 for $A=0.61$, respectively. It is also numerically found that the stabilized inverted SP denoted by the solid line becomes unstable for a second critical value $A^*_{\mathrm{nu},2}$ $(=0.529\,159\ldots)$ through a period-doubling bifurcation, giving rise to the birth of a symmetric orbit of period 2 denoted by the solid line.

We also carry out the above experiments for many other values of Ω, and thus measure the first and second critical values, $A^*_{\mathrm{expt},1}$'s and $A^*_{\mathrm{expt},2}$'s. Figure 7 shows the stability diagram of the inverted SP. The experimental data for $A^*_{\mathrm{expt},1}$ and $A^*_{\mathrm{expt},2}$ are represented by the open and solid circles, respectively. The inverted SP is observed to become stable in the interval between $A^*_{\mathrm{expt},1}$ and $A^*_{\mathrm{expt},2}$. Note also that the width of this interval becomes smaller as Ω is increased. Hence the stabilization of the inverted SP can be more easily observed for small values of Ω, compared to the cases of high Ω values. For a comparison with the experimental results, numerical data obtained using the Floquet theory are also given in Fig. 7. The lower stability boundary $A^*_{\mathrm{nu},1}$ denoted by the dashed line is a subcritical pitchfork bifurcation line, while the upper stability boundary $A^*_{\mathrm{nu},2}$ denoted by the solid line is a period-doubling bifurcation line. We note that the agreement between the experimental and numerical results becomes better as Ω is decreased.

IV. SUMMARY

Bifurcations of normal and inverted SP's in the parametrically forced magnetic pendulum are experimentally studied by varying the two parameters Ω and A. As A is increased above a critical value, the normal SP is observed to become unstable either by a period-doubling bifurcation or by a symmetry-breaking pitchfork bifurcation, depending on the values of Ω. In the 1st range I of Ω (i.e., $0.2\leqslant\Omega\leqslant0.5$), a new stable symmetric orbit with period 2 appears via period-doubling bifurcation, while a conjugate pair of new stable asymmetric orbits with period 1 is born via symmetry-breaking pitchfork bifurcation in the second range II of Ω (i.e., $0.8\leqslant\Omega\leqslant1.025$). However, in contrast to this normal SP, the inverted SP is observed to become stable when A is increased above a first critical value A^*_1 by a subcritical pitchfork bifurcation. Unfortunately a pair of asymmetric orbits of period 1 born for this subcritical case cannot be ex-

perimentally observed, because they are unstable ones. As A is further increased, the stabilized inverted SP is also observed to lose its stability for a second critical value A_2^* by a period-doubling bifurcation, giving rise to the birth of a new stable symmetric period-doubled orbit. Thus the inverted SP becomes stable in the interval between A_1^* and A_2^*. When all of these experimental results for the two SP's are compared with the numerical results obtained using the Floquet theory, they seem to agree well.

ACKNOWLEDGMENTS

This work was supported by the Basic Science Research Institute Program, Ministry of Education, Korea, Project No. BSRI-96-2401.

[1] V. Croquette and C. Poitou, J. Phys. (France) Lett. **42**, 537 (1981).
[2] H. Meissner and G. Schmidt, Am. J. Phys. **54**, 800 (1986).
[3] K. Briggs, Am. J. Phys. **55**, 1083 (1987).
[4] V. I. Arnold, *Mathematical Methods of Classical Mechanics* (Springer-Verlag, New York, 1978), p. 113.
[5] J. B. McLaughlin, J. Stat. Phys. **24**, 375 (1981).
[6] R. W. Leven and B. P. Koch, Phys. Lett. A **86**, 71 (1981).
[7] S.-Y. Kim and K. Lee, Phys. Rev. E **53**, 1579 (1996).
[8] B. P. Koch, R. W. Leven, B. Pompe, and C. Wilke, Phys. Lett. A **96**, 219 (1983).
[9] R. W. Leven, B. Pompe, C. Wilke, and B. P. Koch, Physica D **16**, 371 (1985).
[10] J. Guckenheimer and P. Holmes, *Nonlinear Oscillations, Dynamical Systems, and Bifurcations of Vector Fields* (Springer-Verlag, New York, 1983), p. 24.
[11] J. J. Stoker, *Nonlinear Vibrations in Mechanical and Electrical Systems* (Interscience, New York, 1950), p. 189.
[12] H. C. Corben and P. Stehle, *Classical Mechanics*, 2nd ed. (Wiley, New York, 1960), p. 66.
[13] P. L. Kapitza, in *Collected Papers by P.L. Kapitza*, edited by D. Ter Haar (Pergamon, London, 1965), Vol. 2, p. 714.
[14] V. I. Arnold, *Mathematical Methods of Classical Mechanics* (Springer-Verlag, New York, 1978), p. 121.
[15] J. A. Blackburn, H. J. T. Smith, and N. Grøbech-Jensen, Am. J. Phys. **60**, 903 (1992); H. J. T. Smith and J. A. Blackburn, *ibid.* **60**, 909 (1992).
[16] By decreasing the value of $B_{\rm dc}$ from some positive value, we first obtain a data set of $\omega_0(B_{\rm dc})$ for several values of $B_{\rm dc}$ through the fitting procedure described in the fourth paragraph in Sec. II. We can then obtain the values of $B_{E,n}$ and m/I by fitting the experimental data set of $\omega_0(B_{\rm dc})$ to the equation, $\omega_0=\sqrt{(m/I)(B_{\rm dc}+B_{E,n})}$.
[17] S. Lefschetz, *Differential Equations: Geometric Theory* (Dover, New York, 1977), p. 60.
[18] J. Guckenheimer and P. Holmes, *Nonlinear Oscillations, Dynamical Systems, and Bifurcations of Vector Fields* (Springer-Verlag, New York, 1983), Sec. 3.5.